Applied Catalysis A: General 475 (2014) 282–291

Contents lists available at ScienceDirect

Applied Catalysis A: General

journal homepage: www.elsevier.com/locate/apcata

Liquid-phase hydrogenation of acetophenone over silica-supported Ni, Co and Cu catalysts: Influence of metal and solvent

A.F. Trasarti, N.M. Bertero, C.R. Apesteguía, A.J. Marchi *

Catalysis Science and Engineering Research Group (GICIC), Instituto de Investigaciones en Catálisis y Petroquímica (INCAPE), UNL-CONICET, Santiago del Estero 2654, 3000, Santa Fe, Argentina

ARTICLE INFO

Article history:
Received 19 November 2013
Received in revised form 9 January 2014
Accepted 17 January 2014
Available online 27 January 2014

Keywords:
Hydrogenation
Acetophenone
1-Phenylethanol
Solvent effect
Metal-based catalysts

ABSTRACT

In this work, we studied the influence of solvent and metal nature on the liquid-phase hydrogenation of acetophenone (AP) over Ni/SiO_2, Co/SiO_2 and Cu/SiO_2. Catalysts were prepared by wetness impregnation method with metal loads of about 7–8 wt%. Catalytic tests were performed in a batch reactor, at 363 K and 10 bar (H_2), using 2-propanol (IPA), cyclohexane (CHX), toluene (TOL) and benzene (BEN) as solvents. Considering the three catalysts, the general pattern for the initial hydrogenation rate was: $Ni/SiO_2 > Co/SiO_2 > Cu/SiO_2$, whereas the trend for selectivity to 1-phenylethanol (PHE) was just the opposite. AP can interact with nickel metal surface through both –C=O group and aromatic ring and thus the aromatic alcohol and saturated compounds were obtained. Instead, cobalt and copper metal surfaces interact preferentially with the –C=O group leading to selective hydrogenation of AP into PHE. In addition, an important interaction between –C–OH group of PHE and Co/SiO_2 surface takes place, leading to rapid alcohol hydrogenolysis into ethylbenzene. The general activity pattern with the four solvents was: IPA > CHX ≥ TOL ≥ BEN. The magnitude of solvent influence on the catalytic performance strongly depended on the metal nature. The most significant solvent effect took place with Ni/SiO_2, whereas the less noticeable influence was observed in the case of Cu/SiO_2. From pseudo-homogenous kinetic modeling and temperature-programmed desorption, the following noteworthy observations arose: (1) IPA has a positive contribution by hydrogen transfer and/or AP activation by polarization; (2) the magnitude of the positive IPA influence on AP hydrogenation rate follows the trend: $Ni/SiO_2 > Co/SiO_2 > Cu/SiO_2$; (3) CHX has a neutral contribution because of its weak adsorption on the metal phase and low interaction with reactant and products; (4) the effect of TOL and BEN is clearly negative for Ni/SiO_2 due to blockage of active sites by strong adsorption of solvent on the metallic surface; (5) the effect due to strong adsorption of TOL and BEN is much less noticeable on Co/SiO_2 and Cu/SiO_2, as a consequence, the pattern for AP hydrogenation rates in BEN and TOL is $Cu/SiO_2 > Co/SiO_2 > Ni/SiO_2$. Selectivity to PHE was less influenced by solvent nature. However, in the case of Ni/SiO_2 and Co/SiO_2, maximum PHE yields and selectivities increased with the solvent–metal interactions, mainly due to inhibition of the PHE hydrogenolysis. Cu/SiO_2 was always 100% selective to PHE in all of the solvents. These results are clearly indicating that the magnitude of the solvent effect on catalytic performance strongly depends on the metal nature.

1. Introduction

Selective hydrogenation of carbonyl compounds to the corresponding alcohols is of great importance in Fine Chemistry and pharmaceutical industry. In particular, selective hydrogenation of aromatic ketones into the corresponding alcohols is of interest because the reaction products are widely used as flavors and fragrances, as well as intermediates for the synthesis of valuable organic molecules [1]. Hydrogenation of aromatic ketones is also interesting from a basic point of view because it involves a challenging problem of chemo- and regioselectivity; in addition to the usually desired hydrogenation of the carbonyl group, other side reactions can occur, as the aromatic ring hydrogenation and hydrogenolysis of the corresponding alcohols [2].

The hydrogenation of acetophenone (AP) is particularly important because of the extensive industrial use of 1-phenylethanol (PHE), which finds application in the pharmaceutical and fragrance industries [1]. The general reaction network, with all the possible reaction pathways during AP hydrogenation, is depicted in Fig. 1. Hydrogenation of carbonyl group of AP gives PHE, whereas the hydrogenation of the aromatic ring leads to

* Corresponding author. Tel.: +54 342 4571164; fax: +54 342 4531068.
E-mail addresses: amarchi@fiq.unl.edu.ar, albertojuliomarchi@gmail.com (A.J. Marchi).

0926-860X/$ – see front matter © 2014 Elsevier B.V. All rights reserved.
http://dx.doi.org/10.1016/j.apcata.2014.01.038

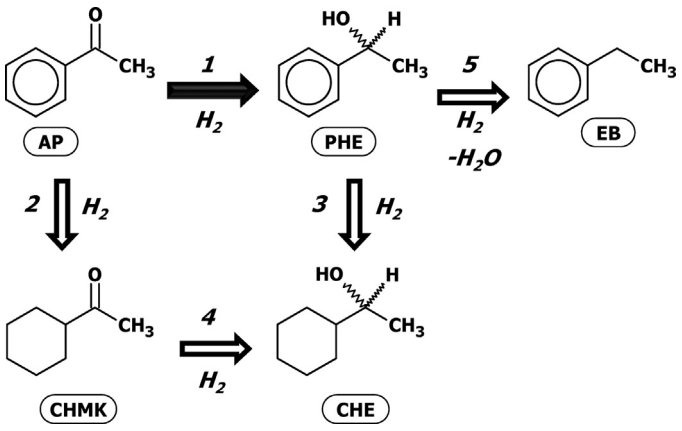

Fig. 1. Reaction scheme for acetophenone hydrogenation over metal catalysts. AP: acetophenone. PhE: 1-phenylethanol. CHMK: cyclohexylmethylketone. CHE: cyclohexanol; EB: ethylbenzene.

cyclohexylmethylketone (CHMK). Both primary products, PHE and CHMK, can subsequently be hydrogenated to 1-cyclohexylethanol (CHE). The hydrogenolytic splitting of the C–OH bond of PHE produces ethylbenzene (EB).

Earlier studies at various temperatures and pressures were performed over supported Pd, Pt, Ni, Cu and Ru catalysts [3–19]. The product distribution was strongly dependent on the metal catalyst and reaction conditions. Hydrogenation of AP over Pt-based catalysts produces important amounts of CHMK and CHE as by-products [3,4]. Ru-based catalysts showed a similar behavior to that of Pt-based catalysts, with high activity to hydrogenate the aromatic ring [5,6]. In contrast, a consecutive reaction path comprising the hydrogenation of AP to PHE and hydrogenolysis to EB has been reported with Pd catalysts [7–9]. An intermediate behavior was observed with bulk and supported Ni catalysts [10–16]. Besides, a very important solvent effect on the catalytic activity was determined when Ni-based catalysts are employed for the AP hydrogenation in liquid-phase [17]. There are few works reporting the use of Cu catalysts in this reaction [18–21], though this metal seems to be very selective to the aromatic alcohol. On the other hand, to our knowledge, the use of Co-based catalysts in the liquid-phase hydrogenation of AP was reported only once, showing a high activity for C–OH hydrogenolysis [22].

Although the selection of the metal is a very important step to achieve both high activity and selectivity to the valuable product in the process, the solvent selection is of great relevance, as well. In a previous work, we have demonstrated the influence of the solvent on the catalytic activity and selectivity for the AP hydrogenation over Ni/SiO_2 catalyst [17]. In that work, a deep analysis of the effect of the solvent/reactant and solvent/catalyst interactions on the catalytic activity was carried out. It was found that solvent/metal interactions are crucial for the performance of Ni/SiO_2 catalyst in the liquid phase hydrogenation of AP. However, it is expected that the magnitude of these interactions will depend on the metal nature. The aim of this work is to get a more extended vision about the influence of the solvent on the hydrogenating performance of a metal by using different non-noble metal catalysts. To achieve this objective, the AP hydrogenation was studied over silica-supported Ni-, Co- and Cu-based catalysts, performing the liquid phase reaction in four selected solvents. The four solvents were chosen according to their abilities to interact with the catalysts and the reactant. The solvent–catalyst interactions were studied by temperature-programmed desorption of the solvents and fitting the catalytic activity tests by applying a pseudo-homogeneous kinetic model. On the basis of the results obtained in this work, we proposed an explanation for the solvent effect on the catalytic activity depending on the metal nature.

2. Experimental

2.1. Catalyst preparation

Ni, Co and Cu silica-supported catalysts were prepared with metal loadings of about 8 wt%. The metals were deposited on commercial silica (Grace G62, 99.7%, $S_g = 230\ m^2/g$, $V_p = 1.19\ cm^3/g$) by incipient wetness impregnation from aqueous solutions of 0.57 M $Ni(NO_3)_2$, $Co(NO_3)_2$ or $Cu(NO_3)_2$. The solids were subsequently dried in an oven at 373 K for 12 h, followed by calcination in air flow at 673 K for 3 h. Previously to the catalytic test, samples were activated ex-situ in H_2 flow (60 cm^3/min) for 2 h and then charged into the reactor under inert atmosphere of N_2, in order to avoid metal re-oxidation.

2.2. Characterization of the catalysts

The polycrystalline structures of the samples were identified by X-ray diffraction (XRD) using a Shimadzu XD-1 diffractometer, Ni-filtered Cu $K\alpha$ radiation and a scan speed of 2°/min. The average crystallite sizes of metal oxides were estimated by applying the Scherrer equation.

BET surface area (S_g) and mean pore diameter (d_P) were measured by N_2 physisorption at 77 K in a Quantochrome Corporation NOVA-1000 sorptometer. Elemental compositions were measured by atomic absorption spectroscopy (AAS) using a Perkin-Elmer 3110 spectrophotometer.

The reducibility of the calcined samples was determined by temperature programmed reduction (TPR). The TPR profiles were obtained in a stream of H_2 (5%)/Ar (60 cm^3/min), while raising the temperature from 298 to 773 K at 10 K/min and monitoring the H_2 consumption using a TCD detector.

In order to measure the metallic dispersion on Cu/SiO_2, the dissociative adsorption of N_2O was used [23]. Sample was previously reduced in H_2 flow at 543 K for 2 h and then the system was evacuated in Ar flow during 30 min. After cooling down the reactor up to 363 K, pulses of N_2O (10%)/Ar were fed to the sample bed. The evolution of these pulses was followed by mass spectrometry using a Baltzers Omnistar unit. Metal copper dispersion was calculated from N_2O uptake assuming the stoichiometry of reaction (1).

$$N_2O(g) + 2Cu^0(s) \Rightarrow N_2(g) + Cu_2O(s) \quad (1)$$

The metallic dispersion of Ni/SiO_2 was determined by hydrogen chemisorption. Volumetric adsorption experiments were performed at 298 K in a conventional volumetric apparatus, using the double-isotherm method (0–0.066 bar) as described elsewhere [24]. Ni/SiO_2 was reduced in H_2 at 673 K for 2 h and then outgassed 2 h at this temperature under vacuum before gas chemisorption experiments. A stoichiometric atomic ratio of H/Ni = 1 was used to estimate the nickel dispersion.

2.3. Catalytic tests

Hydrogenation of AP was carried out in liquid phase using a 600 ml autoclave (Parr 4843) equipped with mechanic stirrer. The experiments were performed at 363 K, 10 bar (H_2) and with an initial AP concentration of 0.17 M, using 2-propanol (IPA, 99.5% Sigma-Aldrich), cyclohexane (CHX, 99.5% Sigma-Aldrich), toluene (TOL, 99.8% Sigma-Aldrich) and benzene (BEN, 99.5% Merck) as solvents.

An amount of 150 ml of solvent and 0.5–1 g of catalyst (activated ex-situ in 60 cm^3/min H_2 flow for 2 h at 673 K for Ni and Co

and 543 K for Cu) was charged under N_2 inert atmosphere to the autoclave. The reactor was then closed and the stirring was started. Afterwards, the autoclave was heated up to the reaction temperature. Once the reaction temperature was reached, 3.0 ml of AP (99%, Aldrich) was injected into the reactor and then hydrogen was fed until the final pressure value. Stirring speeds of 700 RPM and particle diameters lower than 100 μm were used to avoid external and intraparticle mass transfer limitations. These parameters were fixed on the basis of experimental determinations carried out in previous works [17,21]. In addition, for all of the cases, the quantitative criterion described by Ramachandran and Chaudhari was applied to analyze the significance of gas–liquid, liquid–solid and intraparticle mass transfer on the reaction kinetics [25]. This criterion has been widely employed for liquid-phase hydrogenation reactions [14,17]. The absence of intraparticle diffusion limitations was also checked by using the Weisz-Prater criterion [26]. On the basis of the above analysis, it was verified that in this work the rate data were obtained under chemical regime.

The concentrations of AP and reaction products were followed during the experiments by ex-situ gas chromatography using an Agilent 6850 chromatograph equipped with flame ionization detector (heated at 523 K), temperature programmer, and a 30 m Innowax capillary column with a 0.25 μm coating. The analysis was carried out between 363 and 393 K with a heating rate of 10 K/min. The injector temperature was set at 523 K.

Liquid samples were withdrawn from the reactor by using a loop under pressure in order to avoid flushing of liquid samples. Reactant conversion (X_{AP}, mol of AP reacted/mol of AP fed) was calculated as $X_{AP} = \left(C^0_{AP} - C_{AP}\right)/C^0_{AP}$, where $C^0{}_{AP}$ is the initial concentration of acetophenone and C_{AP} is the acetophenone concentration at reaction time t. Product yields (η_j, mol of product j/mol of AP fed) were calculated as $\eta_j = C_j/C^0_{AP}$.

2.4. Temperature-programmed desorption experiments

The nature and strength of the solvent/catalyst interactions were studied by temperature-programmed desorption (TPD) of solvents pre-adsorbed at 298 K. Calcined samples (150 mg) were activated in a 60 cm^3/min flow of H_2 (5%)/Ar (as described in Section 2.3) and then cooled down up to 298 K. Afterwards, a He stream was bubbled through the solvent in order to saturate the gaseous stream with solvent vapor. Then, the reduced sample was exposed to this stream for 15 min following the effluent composition by mass spectrometry (MS) in a Baltzers Omnistar unit. After this adsorption period, the catalyst was exposed to a He stream (60 cm^3/min) at room temperature for 1 h, with the purpose of removing the physisorbed solvent. Finally, the catalyst temperature was increased at 10 K/min and the composition of the reactor effluent was monitored by mass spectrometry (MS).

In some selected cases, temperature-programmed hydrogenation (TPH) was carried out in a flow of H_2 (5%)/Ar (60 cm^3/min) with the aim of favoring the desorption of strongly adsorbed unsaturated species, in order to obtain additional information to that obtained by TPD. These experiments were performed as described above for TPD experiments.

3. Results

3.1. Catalyst characterization

The results of catalyst characterization by different techniques are given in Table 1. In all of the cases, the metal load was about 7–8 wt%. The BET surface area of the supported catalysts did not differ significantly from the silica support (230 m^2/g), indicating

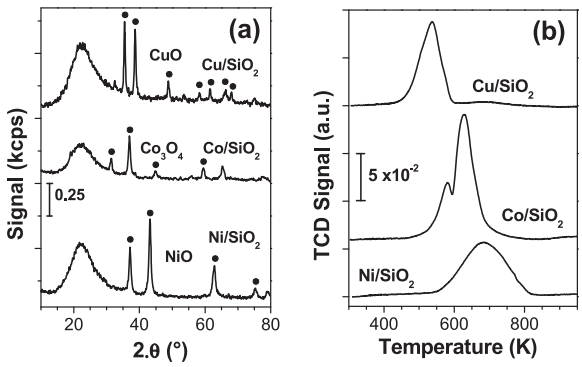

Fig. 2. Characterization of the catalytic samples: (a) XRD pattern of the calcined samples; (b) TPR profiles of the calcined samples.

that the impregnation process did not modify to a considerable extent the textural properties of the support.

After decomposing the metal nitrate precursors by calcinations in air at 673 K, samples were characterized by XRD and the results are shown in Fig. 2a. Only polycrystalline NiO (JCPDS 47-1049), Co_3O_4 (JCPDS 78-1970) and CuO (JCPDS 01-080-1268) were identified on Ni/SiO_2, Co/SiO_2 and Cu/SiO_2, respectively. The mean crystallite size of these oxides was estimated by applying the Scherrer equation and the results are summarized in Table 1. In all of the cases, the estimated values were between 13 and 19 nm. As a consequence, in all of the samples, the metal oxide phase deposited on the silica surface was formed by large particles, even if crystallite agglomeration did not take place.

Profiles obtained by TPR (Table 1 and Fig. 2b) showed that reduction of NiO and CuO on silica gives rise to single broad peaks centered at 679 and 536 K, respectively. Each profile corresponds to the direct reduction of NiO and CuO to Ni^0 and Cu^0, in agreement with the identification by XRD (Fig. 2a) and results obtained in previous works [17,21]. The TPR profile of Co_3O_4 on silica exhibited two broad H_2 consumption peaks with maxima at 578 and 628 K, which reflect the consecutive reduction of Co^{3+} ions in two steps, as follows: (1) Co^{3+} into Co^{2+}; 2) Co^{2+} into Co^0 [27]. On the basis of the TPR results, and for the catalysts used in this work, it is inferred that the Ni, Co and Cu fractions are totally converted to the metallic state after the reduction step performed previously to the catalytic tests.

The metallic fraction of reduced catalysts was characterized by hydrogen chemisorption (Table 1). The pattern obtained for the volume of irreversible chemisorbed H_2 was the following: Ni > Co > Cu. The obtained values show that the metal capability for irreversible H_2 chemisorption varies around one order from Ni/SiO_2 to Cu/SiO_2.

The amount of irreversible chemisorbed H_2 was used to estimate the nickel dispersion on Ni/SiO_2, applying a H:Ni = 1 stoichiometry. Assuming a cubic geometry for the metal particles, a nickel dispersion of 3% was determined. It is known that the H_2 chemisorption is not suitable for determining the metal dispersion of Cu and Co-based catalyst [28]. The metal dispersion of Cu, determined by the dissociative adsorption of N_2O at 363 K, was about 2%. These results are consistent with the large crystallite size estimated by applying the Scherrer equation for the corresponding oxide precursors.

The low dispersions obtained for the metallic samples are in good agreement with usual dispersion values for silica-supported metal catalysts prepared by incipient wetness impregnation [22,28,29].

3.2. Catalytic tests

The catalytic activity of Ni/SiO_2, Co/SiO_2 and Cu/SiO_2 was studied and analyzed using four solvents: IPA, CHX, TOL and BEN,

Table 1
Physicochemical characterization of the oxide precursors and reduced samples employed in the liquid-phase acetophenone hydrogenation.

Catalyst	Metal loading (%)	Polycrystalline oxide[a]	Crystallite size[b] (nm)	TPR T_{MAX} (K)	S_g (m^2/g)	Irreversible chemisorbed H_2 (l_{STP}/mol_{Me})
Ni/SiO_2	7.6	NiO	13.5	679	245	0.71
Co/SiO_2	7.7	Co_3O_4	13.1	578, 628	240	0.16
Cu/SiO_2	6.8	CuO	19.0	536	220	0.08

[a] Identified by XRD after thermal decomposition.
[b] Estimated by the Scherrer's equation.

which are commonly used in fine-chemistry hydrogenation reactions. These solvents were chosen from a previous work [17] where it was concluded that they interact with the metal surface in different modes and with varying intensity. The evolutions of reactant conversion with $W{\cdot}t/n^0_{AP}$, over the three metal catalysts and with the four solvents, are shown in Fig. 3. It is clear that, for a given solvent, the intensity of the solvent effect depends on the metal nature, affecting the metal hydrogenation activity in different ways. In order to analyze the metal and solvent effects on the AP hydrogenation activity, the corresponding initial hydrogenation rates (r^0_{AP}) were estimated from these evolutions applying: (1) polynomial interpolation and numerical differentiation at zero time; (2) kinetic modeling. In order to establish the mathematical kinetic model, it was considered that the only reaction products detected in all of the cases were PHE, CHMK, CHE and EB (Fig. 4), which is in agreement with the scheme shown in Fig. 1. Due to the fact that this general reaction scheme is valid for the three catalysts, the catalytic activity data were fitted using a first-order pseudo-homogeneous kinetic model, represented by Eqs. (1)–(5), where $C_i^* = C_i/C^0_{AP}$.

$$\frac{dC^*_{AP}}{dt} = \frac{1}{C^0_{AP}} \times \frac{dC_{AP}}{dt} = -(k_1 + k_2) \times C^*_{AP} \quad (1)$$

$$\frac{dC^*_{PHE}}{dt} = \frac{1}{C^0_{AP}} \times \frac{dC_{PHE}}{dt} = k_1 \times C^*_{AP} - k_3 \times C^*_{PHE} - k_5 \times C^*_{PHE} \quad (2)$$

$$\frac{dC^*_{CHMK}}{dt} = \frac{1}{C^0_{AP}} \times \frac{dC_{CHMK}}{dt} = k_2 \times C^*_{AP} - k_4 \times C^*_{CHMK} \quad (3)$$

$$\frac{dC^*_{CHE}}{dt} = \frac{1}{C^0_{AP}} \times \frac{dC_{CHE}}{dt} = k_3 \times C^*_{PHE} + k_4 \times C^*_{CHMK} \quad (4)$$

$$\frac{dC^*_{EB}}{dt} = \frac{1}{C^0_{AP}} \times \frac{dC_{EB}}{dt} = k_5 \times C^*_{PHE} \quad (5)$$

The system of differential Eqs. (1)–(5) was solved numerically by using the Runge–Kutta–Merson algorithm. The numerical and statistical analyses were carried out as detailed in a previous work [21]. In all of the cases, a satisfactory fitting was obtained, from both physical and statistical point of view. The k_i values (i = 1–5) were significantly different from zero for a confidence interval of 95%. Therefore, k_i values, shown in Table 2, are representative for estimating hydrogenation rates and selectivities. The estimated values for the initial AP hydrogenation rate $\left[r^0_{AP} = (k_1 + k_2) \times C^0_{AP} \times \left(V_T/W_C\right)\right]$ and the initial selectivity to PHE $\left[S^0_{PHE} = k_1/(k_1 + k_2) \times 100\right]$ are also shown in Table 2 for the three metal catalysts and the four solvents.

3.2.1. Metal effect

Based on the fact that SiO_2 is a non-reactive support and the interaction between the large metal crystallites and the SiO_2 is weak, it is expected that AP hydrogenation over M/SiO_2 will take place via a monofunctional mechanism on metallic sites [2].

With the aim of studying the metal effect on AP hydrogenation, CHX was selected as solvent due to its very weak interaction with both metal surface and reactant molecules [17]. It is clear that the metal nature has a strong effect on both activity and selectivity to PHE (Figs. 3 and 4, Table 2). Comparing the catalytic activity results, the resulting pattern is: $Ni/SiO_2 > Co/SiO_2 > Cu/SiO_2$. This pattern is in good agreement with the trend found for irreversible chemisorption of H_2 (Table 1), suggesting that, in absence of solvent-catalyst interactions, differences in catalytic activity can be related with the capability of each metal for dissociative hydrogen chemisorption.

The evolutions of the reactant and product concentrations with the three metal catalysts in CHX are shown in Fig. 4. On Ni/SiO_2, the main primary product was PHE, whereas CHMK was produced in minor amounts (Fig. 4a). Small quantities of CHE and EB were also observed. With all of the solvents, k_1 estimate was at least one order of magnitude higher than k_2 estimate, obtaining initial selectivities to PHE higher than 93.5% (Table 2). In summary, hydrogenation of the aromatic ring and hydrogenolysis of PHE take place over Ni/SiO_2, but in a very small extent.

The results obtained with Co/SiO_2 catalyst greatly differed from the Ni/SiO_2, because aromatic ring hydrogenation products (CHMK and CHE) were not observed ($k_2 = k_3 = 0$). Then, PHE was the only primary product ($S^0_{PHE} = 100\%$, Table 2 and Fig. 4b). However, Co/SiO_2 showed a strong hydrogenolytic character in all solvents, converting PHE into EB at high rates ($k_5 > 0$). These results suggest

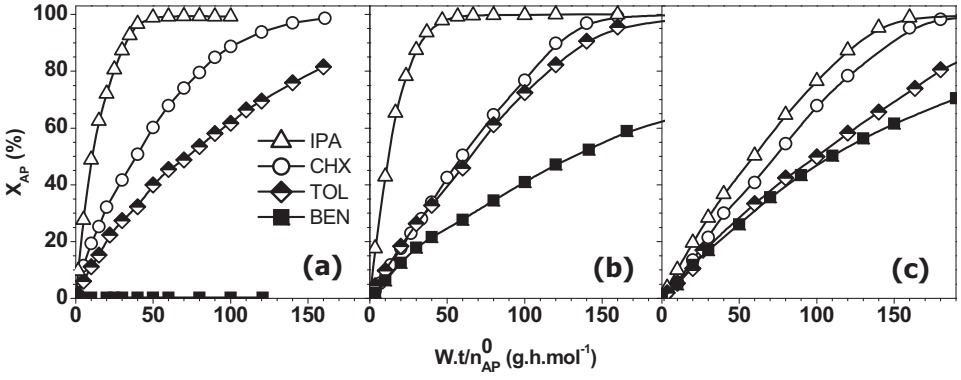

Fig. 3. Solvent effect on the catalytic activity: (a) Ni/SiO_2; (b) Co/SiO_2; (c) Cu/SiO_2 [T = 363 K, p_{H_2} = 8.7 bar, W = 0.5–1 g, C^0_{AP} = 0.17 M, V_{SOLV} = 150 ml, 600 RPM].

Table 2
Initial AP hydrogenation rates, kinetic constants, initial selectivity to PHE and maximum yield in PHE over Ni/SiO_2, Co/SiO_2 and Cu/SiO_2 with the four solvents [T = 363 K, p_{H_2} = 8.7 bar, AP/Solvent = 3:150 (ml), W = 0.5 g (Ni/SiO_2) or 1.0 g (Co/SiO_2 and Cu/SiO_2)].

Catalyst	Solvent	r^0_{AP} [a] (mol/h/g)	r^0_{AP} [b] (mol/h/g)	k_1 [b] (h^{-1})	k_2 [b] (h^{-1})	k_5 [b] (h^{-1})	S^0_{PHE} [c] (%)	η^M_{PHE} [d] (%)
Ni/SiO_2	IPA	6.54×10^{-2}	6.66×10^{-2}	1.27 ± 0.03	$2.45 \times 10^{-2} \pm 4.41 \times 10^{-3}$	$2.42 \times 10^{-2} \pm 5.32 \times 10^{-3}$	98.1	92.3
	CHX	1.75×10^{-2}	1.78×10^{-2}	0.32 ± 0.02	$2.24 \times 10^{-2} \pm 5.53 \times 10^{-3}$	$9.84 \times 10^{-3} \pm 1.16 \times 10^{-3}$	93.5	85.6
	TOL	1.22×10^{-2}	1.03×10^{-2}	0.19 ± 0.01	$7.56 \times 10^{-3} \pm 2.08 \times 10^{-3}$	$2.62 \times 10^{-2} \pm 3.67 \times 10^{-3}$	96.2	88.1
	BEN	0	–	–	–	–	–	–
Co/SiO_2	IPA	5.44×10^{-2}	5.53×10^{-2}	2.11 ± 0.04	0	$9.48 \times 10^{-2} \pm 4.92 \times 10^{-3}$	100	63.2
	CHX	1.13×10^{-2}	9.94×10^{-3}	0.44 ± 0.02	0	$0.14 \pm 1.24 \times 10^{-2}$	100	38.5
	TOL	1.05×10^{-2}	1.03×10^{-2}	0.41 ± 0.02	0	$0.42 \pm 5.89 \times 10^{-2}$	100	46.8
	BEN	6.36×10^{-3}	6.50×10^{-3}	0.25 ± 0.03	0	$0.12 \pm 2.07 \times 10^{-2}$	100	57.9
Cu/SiO_2	IPA	1.12×10^{-2}	1.13×10^{-2}	0.44 ± 0.02	0	0	100	100
	CHX	6.96×10^{-3}	6.86×10^{-3}	0.27 ± 0.02	0	0	100	100
	TOL	6.90×10^{-3}	6.86×10^{-3}	0.27 ± 0.02	0	0	100	100
	BEN	6.78×10^{-3}	6.61×10^{-3}	0.26 ± 0.03	0	0	100	100

[a] Approximated from experimental data by numerical interpolation and differentiation.
[b] Estimated with the pseudo-homogeneous kinetic model by $r^0_{AP} = (k_1 + k_2) \times C^0_{AP} \times \left(V_T / W_C\right)$.
[c] Initial PHE selectivity calculated as $S^0_{PHE} = k_1/(k_1 + k_2) \times 100$.
[d] Maximum yield in PHE during the run.

that Co/SiO_2 is more hydrogenolytic than Ni/SiO_2, but it has a lower tendency to hydrogenate the aromatic ring.

Finally, Cu/SiO_2 was totally selective to PHE, with no formation of CHMK, CHE and/or EB (Fig. 4c and Table 2), in agreement with previous results [21]. Because of this, for the Cu/SiO_2 catalyst, the only estimate that was significantly different from zero is k_1 (Table 2).

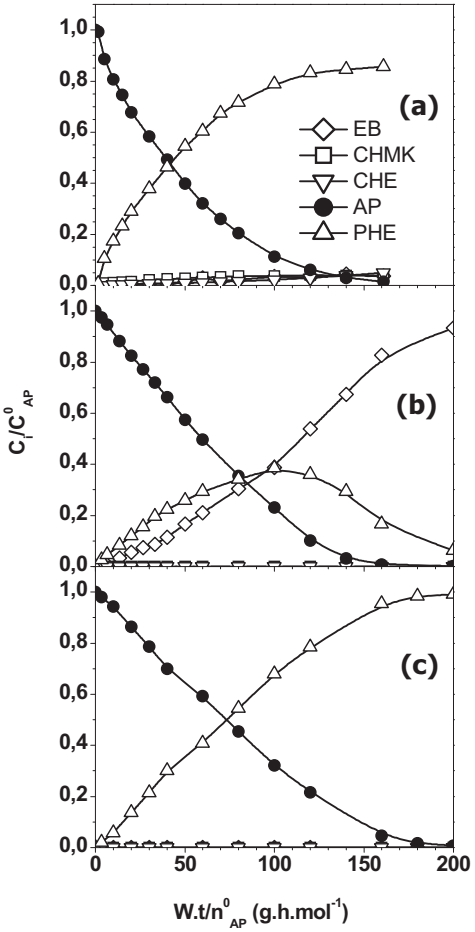

Fig. 4. Evolution of the concentration of AP and products as a function of $W \cdot t/n^0_{AP}$ for the three metal catalysts: (a) Ni/SiO_2; (b) Co/SiO_2; (c) Cu/SiO_2 [T = 363 K, p_{H_2} = 8.7 bar, W = 0.5–1 g, C^0_{AP} = 0.17 M, V_{SOLV} = 150 ml (CHX), 600 RPM].

3.2.2. Solvent effect

From the analysis of Fig. 3 and Table 2, two remarkable observations arise: (1) there is an important influence of the solvent on the AP hydrogenation rate, in such a way that the general activity pattern observed was: IPA > CHX ≥ TOL ≥ BEN; (2) the magnitude of the solvent effect is strongly depending on the metal nature, noting the most remarkable effect with Ni/SiO_2 and the least one with Cu/SiO_2.

In particular, the initial hydrogenation rate over Ni/SiO_2 varied with the solvent according to the following pattern: IPA > CHX > TOL ≫ BEN. Instead, the corresponding pattern with Co/SiO_2 was IPA > CHX ≅ TOL > BEN that changed to IPA > CHX ≅ TOL ≅ BEN over Cu/SiO_2 (Table 2). Besides, r^0_{AP} in IPA and CHX decreased following the pattern: Ni/SiO_2 > Co/SiO_2 > Cu/SiO_2, whereas r^0_{AP} in BEN increased following just the opposite trend (Table 2). Even more, when BEN was used as solvent, no AP hydrogenation was observed with Ni/SiO_2 while an important AP amount was hydrogenated over Co/SiO_2 and Cu/SiO_2. When TOL was used as solvent, Ni/SiO_2 and Co/SiO_2 showed similar initial activity whereas Cu/SiO_2 was the least active of the series. These results strongly suggest that the nature and strength of the solvent/catalyst interactions are strongly depending on the metal. In consequence, the magnitude of the AP-solvent competitive adsorption on the active metal sites could change with the solvent [17].

In general, it was found that the influence of solvent nature on selectivity was less important than on catalytic activity. The initial selectivity to PHE with Co/SiO_2 and Cu/SiO_2 was 100% in all of the cases, while it was always higher than 93% with Ni/SiO_2 (Table 2). In this last case, the highest initial selectivity to PHE was obtained when IPA was used as solvent, which is the most polar solvent of the series. Also, the highest maximum yield in PHE over Ni/SiO_2 was obtained with IPA (Table 2). The 100% initial selectivity to PHE was kept along the run only with Cu/SiO_2, showing that this catalyst has low activity for hydrogenation of the aromatic ring and hydrogenolysis of C–OH group. Instead, the selectivity to PHE with Co/SiO_2 diminished as AP conversion increased, due to hydrogenolysis of the C–OH bond to produce EB. As a consequence, the maximum yield in PHE was always lower than 65%. Besides, an important influence of solvent nature on the PHE hydrogenolysis over Co/SiO_2 was observed. Thus, the following pattern for the maximum PHE yield was observed as a function of the solvent: IPA > BEN > TOL > CHX (Table 2).

3.2.3. Catalytic hydrogen transfer

The variations in the r^0_{AP} with metal, especially when IPA was used as solvent, might be explained from the differences

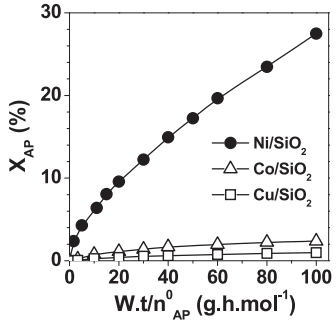

Fig. 5. AP conversion by hydrogen transfer from IPA over the supported metal catalysts [T = 363 K, p_{H_2} = 0 bar, W = 0.5–1 g, C^0_{AP} = 0.17 M, V_{SOLV} = 150 ml, 600 RPM].

in hydrogen chemisorption capacity and hydrogen transfer ability of each metal catalyst. As it was proved in previous works, carbonyl groups can be reduced over supported metal catalysts by hydrogen transfer from secondary and tertiary alcohols in liquid phase [30,31]. In order to evaluate the real capacity of each supported metal catalyst for hydrogen transfer from IPA to AP, a set of catalytic tests in absence of H_2 was performed. The results of these experiments are shown in Fig. 5, where the AP conversion was represented against $W{\cdot}t/n^0_{AP}$ parameter. The pattern for the AP conversion by hydrogen transfer from IPA was: $Ni/SiO_2 \gg Co/SiO_2 \cong Cu/SiO_2$. Over Ni/SiO_2 the AP conversion reached almost 30% after 5 h, whereas in the case of Co/SiO_2 and Cu/SiO_2 the AP conversion by hydrogen transfer was always lower than 5%. The initial hydrogen transfer rate, estimated by numerical interpolation from experimental data, was 7.21×10^{-3}, 7.10×10^{-4} and 2.49×10^{-4} mol/h/g for Ni, Co and Cu based catalysts, respectively. This means that the positive contribution by hydrogen transfer to the global hydrogenation rate is more important over Ni/SiO_2, where r^0_{AP} by hydrogen transfer was 11% of the global r^0_{AP}. Over Co and Cu-based catalyst this contribution was only 1.3% and 2.5%, respectively, of the global hydrogenation rate.

3.3. Study of solvent/catalyst interactions by temperature-programmed desorption

The strength and reversibility of the solvent/catalyst interaction on the M/SiO_2 catalysts were studied by temperature-programmed desorption (TPD). In these tests, desorption temperature of the pre-adsorbed solvent was taken as a measure of the strength of adsorption over the metallic sites. In that sense, when the solvent is not desorbed as the original molecule, fragments coming out from its decomposition were observed, indicating that the solvent adsorption over the metallic surface was very strong and irreversible.

Due to the fact the catalysts used in this work were silica-supported metal catalysts, the temperature-programmed desorption of the four solvents was also studied over the solid oxide support in order to know the magnitude and the strength of the solvent-support interactions. In the four cases, only small amounts of solvent were detected desorbing from the SiO_2, always at temperatures lower than 323 K and without decomposition, indicating very weak interaction with the support surface.

3.3.1. TPD of cyclohexane

The results obtained in the TPD experiments with CHX over the three metal catalysts are shown in Fig. 6a–c. The mass spectrum of cyclohexane is characterized by the m/z = 84 signal (not shown), which corresponds to the molecular ion, and the m/z = 56 signal, which is normally the most intense in the fragmentation mass spectrum of this molecule. Then, the TPD of CHX was followed by recording these two former signals. Additional signals, such as m/z = 28 and 44, due to possible fragmentation of the cyclohexane molecule were recorded, as well. Besides, the m/z = 2 signal was followed to count for the possible dehydrogenation of the molecule over metallic surfaces (not shown in Fig. 6a–c). However, no evolutions with time of any of the former fragments over the three metal catalysts were observed during all of these TPD experiments with CHX. This is indicating that CHX adsorption is so weak on the three catalysts that either the amount chemisorbed was negligible or no appreciable amount of CHX remained adsorbed after flowing He at room temperature for 1 h.

3.3.2. TPD of 2-propanol

The results obtained in the TPD experiments with IPA over the three catalysts are shown in Fig. 6d–f. The evolution of IPA from the catalyst surface was followed by monitoring the signals corresponding to m/z = 2, 43 and 45 assigned to H_2, acetone and IPA, respectively. The m/z = 45 signal corresponds to the molecular ion of IPA, whereas the m/z = 43 signal may come from either an IPA fragment or the molecular ion of acetone, which is the dehydrogenation product obtained from IPA over metallic catalysts. The evolution of m/z = 2 signal at the same temperature of m/z = 43 signal can be indicative of a simultaneous IPA dehydrogenation over metallic sites during the experiment.

In the case of Ni/SiO_2, only a small amount of IPA desorbing at 403 K was observed (signal m/z = 45, Fig. 6d). Almost simultaneously to the IPA desorption, two sharp and intense bands corresponding to m/z = 2 and m/z = 43 were observed. Thus, these signals are assigned to H_2 and acetone coming from the IPA dehydrogenation occurring over metallic nickel sites. Two additional bands corresponding to high temperature H_2 evolution were detected at 583 and 783 K, which were accompanied by C_2 and C_3 hydrocarbon fragments (m/z = 28 and m/z = 44, respectively). These evolutions are indicating the presence of surface nickel sites on which IPA adsorbs very strongly. In fact, this adsorption is so strong that it leads to the decomposition of IPA molecule into C_2 and C_3 compounds and H_2 at temperatures higher than 583 K. In such a kind of metal nickel sites, an irreversible IPA adsorption can be expected under the catalytic test conditions; i.e. temperatures lower than 373 K. In summary, the TPD experiment showed that Ni/SiO_2 has at least three different types of sites: (1) metal nickel sites on which IPA chemisorbs reversibly; (2) metal nickel sites where IPA chemisorbed irreversibly and it is dehydrogenated into acetone and H_2; (3) metal nickel sites where IPA chemisorbs irreversibly and very strongly.

In the case of Co/SiO_2 (Fig. 6e), the signals corresponding to IPA (m/z = 45, 43) showed a maximum at 383 K, i.e. at a slightly lower temperature than in the case of Ni/SiO_2. Besides, comparing the relative intensities of the m/z = 45 and 43 signals in Fig. 6d and e, it can be concluded that a higher amount of reversible chemisorbed IPA is desorbed from the Co/SiO_2 than from Ni/SiO_2. Respect to IPA dehydrogenation on Co/SiO_2, the corresponding signals (m/z = 2, H_2 and m/z = 43, acetone) evolved at a higher temperature (443 K) and showed lower intensity than in the case of Ni/SiO_2 (403 K) (Fig. 6d and e). These results suggest that IPA-Co interaction is less important than for IPA-Ni. Besides, similar to the case of Ni/SiO_2, bands between 553 and 773 K were observed for m/z = 2, 28 and 44 that can be attributed to H_2 and C_2 and C_3 hydrocarbon fragments. The last also indicates the presence of metal cobalt sites where IPA chemisorbs irreversibly and very strongly.

Over Cu/SiO_2 the IPA desorption and dehydrogenation processes took place at temperatures some lower than 443 K, similarly to the case of Co/SiO_2, but signals have even a lower intensity (Fig. 6f). The main difference with the former TPD experiments with IPA is that no significant evolutions at temperatures higher than 553 K were observed for m/z = 2, 28 and 44.

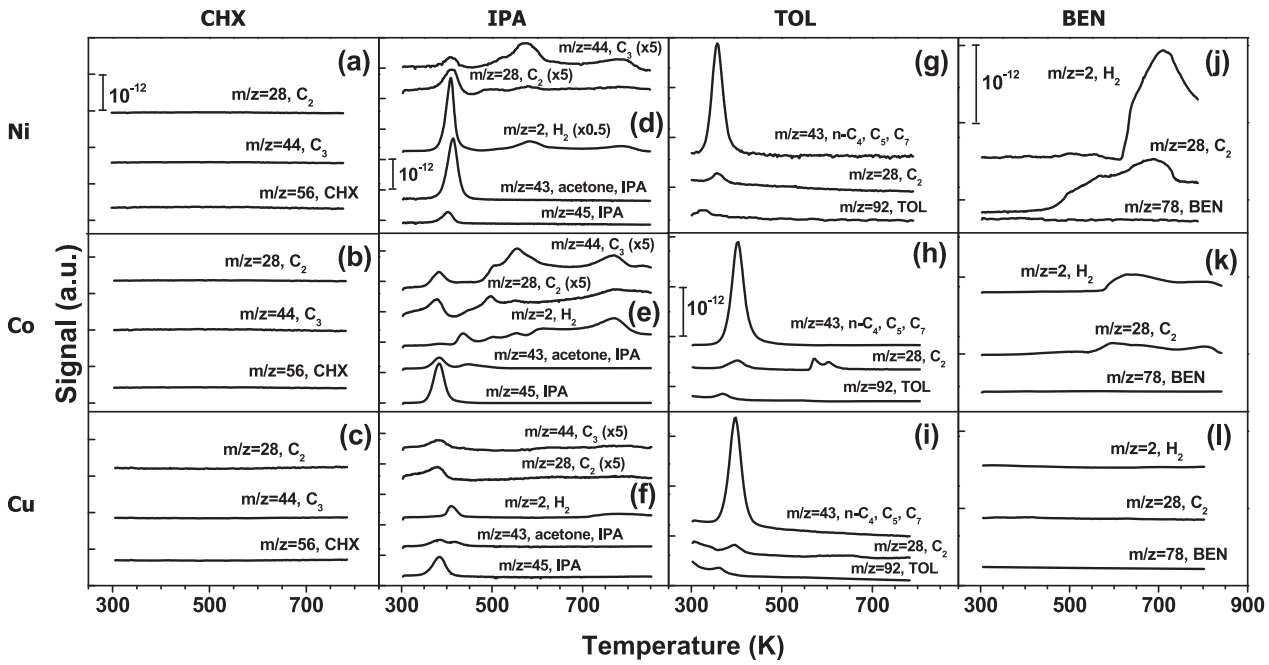

Fig. 6. Temperature-programmed desorption (TPD) of solvents pre-adsorbed at 298 K over silica-supported metal catalysts [He stream (60 cm^3/min), Heating rate: 10 K/min].

In summary, we concluded that both IPA dehydrogenation into acetone and strong irreversible chemisorption diminish according to the following pattern: $Ni/SiO_2 > Co/SiO_2 > Cu/SiO_2$.

3.3.3. TPD of toluene

The results obtained in the TPD experiments with TOL over the three metal-based catalysts are shown in Fig. 6g–i. TOL desorption was followed by recording the $m/z = 92$ signal, corresponding to the molecular ion. Signals $m/z = 28$, 43 and 44 were also followed to count for C_2 and C_4 species.

For the three metal catalysts only a small amount of TOL ($m/z = 92$) desorbed between 323 and 373 K. The main desorption phenomenon occurred between 357 and 407 K involving C_2 and C_4 fragments ($m/z = 28$ and 43). Since these bands were shifted respect to the temperature at which TOL desorbed, these fragments are associated to low temperature TOL decomposition into lighter hydrocarbons. Only in the case of Co/SiO_2, two small bands located at 573 and 603 K, due to high temperature desorption of C_2 ($m/z = 28$), were observed.

In summary, although most of TOL adsorbs irreversibly on all the samples, the TOL decomposition takes place at relatively low temperature.

3.3.4. TPD of benzene

The mass spectrum of BEN is characterized by the $m/z = 78$ signal which corresponds to the molecular ion and other much less abundant fragments. Besides, with similar criterion used in TPD experiments with toluene, signals $m/z = 2$, 28, 43 and 44 were followed to consider any possible BEN decomposition. The results obtained in the TPD of BEN for the three metal catalysts are shown in Fig. 6j–l. From these TPD profiles, it is worth to notice that no BEN desorption ($m/z = 78$) was observed with any of the three samples. Instead, in the case of Ni- and Co-based catalysts, significant evolutions for H_2, C_1 and C_2 species were detected at temperatures higher than 500 K ($m/z = 2$, 16, 28, Fig. 6j and k). These evolutions at high temperatures were attributed to decomposition of strongly chemisorbed BEN over metal nickel and cobalt surfaces. However, from the comparison of these two TPD experiments, it is clear that the amount of H_2 and C_1–C_2 species evolving from Co/SiO_2 is lower than that from Ni/SiO_2, i.e. coverage with strongly adsorbed BEN is occurring in greater extension over metal nickel than over metal cobalt surface.

In contrast with Ni- and Co-based catalysts, neither H_2 nor C_1–C_2 hydrocarbons desorbed from Cu/SiO_2, even at very high temperatures (Fig. 6l). This clearly indicates that interaction between BEN and metal copper surface is much lower than BEN interaction with metal nickel and even with metal cobalt.

In order to obtain more information about the differences in the BEN interaction with metal nickel and cobalt, additional TPH experiments of BEN were performed over the three catalysts.

3.3.5. TPH of benzene

TPH experiments give information about desorption of strongly adsorbed species in the presence of H_2. Fig. 7 shows the corresponding TPH profiles for BEN over the three metal catalysts.

In the case of Ni/SiO_2, very important evolutions for C_1 and C_2 fragments were observed, which took place at temperatures 200 K lower than during TPD experiments (Fig. 6j and Fig. 7a). The complete desorption of C_2 species occurred around 723 K, close to the maximum of the C_2 signal observed during TPD experiment. These shifts to minor temperatures are in agreement with the fact that a high H_2 concentration is favouring hydrogenolysis of BEN strongly adsorbed on metal nickel surface. In the TPH experiment with Co/SiO_2, in line with TPD results, C_1 and C_2 signals were less intense than in the case of Ni/SiO_2 (Fig. 7a and b) and the corresponding evolutions were again observed at temperatures much lower than in the TPD experiment (Fig. 6k and Fig. 7b). A low temperature desorption of C_2 fragments was promoted by H_2 between 350 and 450 K. Besides, a wide but notorious peak for C_1 signal took place at about 500 K; a similar temperature than in the case of Ni/SiO_2 but with a much lower intensity. These results, in agreement with TPD experiments, are clearly indicating that: (1) BEN is strongly adsorbed over metal nickel surface and some metal cobalt sites; (2) BEN interaction with metal cobalt is some weaker than with metal nickel; (3) the amount of BEN adsorbed over metal nickel surface is larger than over metal cobalt surface. In contrast, no evolutions for any hydrocarbon species were observed during

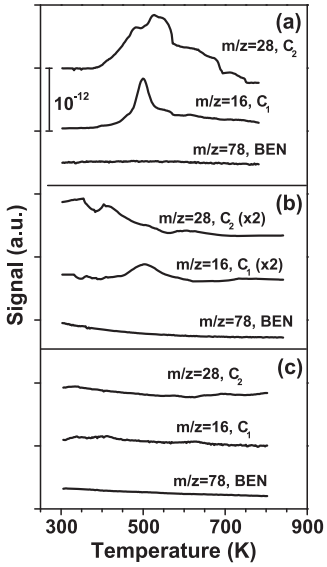

Fig. 7. Temperature-programmed hydrogenation (TPH) of BEN pre-adsorbed at 298 K over silica-supported metal catalysts: (a) Ni/SiO_2; (b) Co/SiO_2; (c) Cu/SiO_2 [H_2 (5%)/Ar (60 cm^3/min), heating rate: 10 K/min].

the TPH experiment with Cu/SiO_2 (Fig. 7c), in agreement with TPD experiment (Fig. 6l).

In summary, the grade of BEN interaction with the three metal catalysts used in this work follows the trend: $Ni/SiO_2 > Co/SiO_2 > Cu/SiO_2$. In addition, BEN coverage is smaller on metal cobalt surface than on metal nickel surface, suggesting that BEN is selectively interacting with only some type of metal cobalt surface sites.

4. Discussion

The results clearly showed a strong influence of the solvent on the AP hydrogenation rate and a significant effect of the metal catalyst on both, the activity and selectivity. Besides, the magnitude of the solvent effect is clearly depending on the metal nature.

The first aspect to be discussed is the metal effect on the hydrogenation rate. From the characterization results, the three metal-based catalysts have similar metal loading and they are all constituted by large metal-supported particles, i.e. all of them have low metallic dispersion. In addition, as a consequence of the preparation method used in this work, the interaction between the metal and the silica-support is weak in all of the catalysts. In order to compare the intrinsic activity of the three metals, minimizing the solvent influence, we decided to contrast the r^0_{AP} values obtained in CHX with each catalyst. This decision was based on the very weak adsorption of CHX on the metallic sites that was known from our previous work [17] and confirmed here from the TPD experiments. The pattern for initial activity in the liquid phase AP hydrogenation was: $Ni/SiO_2 > Co/SiO_2 > Cu/SiO_2$, which is in agreement with the capability for hydrogen chemisorption shown in Table 1. This is indicating that the amount of chemisorbed hydrogen on the metallic surface is important for determining the initial hydrogenation rate.

Regarding the metal effect on the product distribution, important changes in selectivity are observed due to the fact that AP molecule interacts differently with Ni, Co or Cu-based catalysts. Over Ni, AP adsorbs mostly through the C=O group, favoring initial selectivities to PHE higher than 93%. However, some of the reaction products are CHMK and CHE, which are obtained from the aromatic ring hydrogenation [17]. The last is probably coming from AP and PHE adsorbed through the aromatic ring on some metallic sites. In contrast, Co and Cu-based catalyst showed a 100% initial selectivity to PHE. In the case of Co/SiO_2, an important subsequent hydrogenolysis was also observed. Instead, over Cu/SiO_2 no side reactions took place and 100% selectivity to PHE was kept along the whole run, in agreement with previous results [21]. This means that no aromatic ring hydrogenation was observed with Cu/SiO_2 and Co/SiO_2. These results can be explained assuming that repulsion forces overcome the attraction forces between aromatic ring and metal copper or cobalt surfaces [32]. Then, interaction of AP and PHE with metal surface through the C=O and C–OH groups are favored against that through the aromatic ring. Thus, the corresponding hydrogenation and subsequent hydrogenolysis, this last observed only in the case of Co/SiO_2, of AP and PHE are favored against ring hydrogenation. The ratio between repulsion and attraction forces is lower for metal nickel than for metal cobalt and copper. As a consequence, some ring hydrogenation of AP and PHE takes place over Ni/SiO_2. Furthermore, metal nickel and cobalt were more active for both reactions than metal copper probably because metal cobalt and nickel have partially empty *d* bands, which could accommodate more easily the lone pair of electrons of the oxygen atom than when *d* bands are completely filled, as in the case of metal copper.

It is very well known that the hydrogenation reactions in liquid phase over supported-metal catalysts are in general positive order with respect to hydrogen [2,7,14,21]. The fact that the hydrogenation rate increases with H_2 partial pressure when the reaction is carried out in a given solvent reflects the increase of the H_2 concentration in liquid phase according to the Henry' law. When a liquid phase hydrogenation is performed in different solvents at a given temperature and hydrogen pressure, the amount of available H_2 in liquid phase depends only on the H_2 solubility in each solvent. Thus, by reasoning that the hydrogenation reactions are positive order in H_2, it could be expected that the catalyst hydrogenation activity will be higher in solvents providing the highest H_2 solubility [28]. However, this is not always true. For example, we did not find a clear correlation between catalyst activity and H_2 solubility when C1–C3 alcohols were used as solvents in the AP hydrogenation on Ni-based catalysts [17].

Values of H_2 concentration in liquid phase, estimated at the reaction temperature by applying Henry's law, are presented in Table 3 for the solvents used in this work. It can be observed that there is a difference of only around 17% in the H_2 solubility between IPA, a polar compound, and BEN, a non-polar compound, which is not enough to justify the important differences observed in initial hydrogenation rate r^0_{AP} (Table 2). Even more, H_2 is some more soluble in BEN where the hydrogenation rate was always the lowest. Then, it is clear that, besides the positive contribution of H_2 solubility to the hydrogenation activity, other effects rule variations in r^0_{AP} with the solvent. One factor that can affect hydrogenation activity is the solvent-catalyst interaction, as it was showed in a previous work [17].

Other authors have explained the solvent effects on the catalytic activity by considering differences in solvent polarity [7,33]. In a previous work, for solvents of a given family, we have observed that the AP hydrogenation rate on Ni catalysts diminishes with the solvent polarity [17]. For the four solvents used in this work, several polarity parameters and scales are presented in Table 3 [33–37]. In this work, no correlation was found between r^0_{AP} estimates and these polarity parameters, i.e. it was not possible to match the tendencies in polarity with the r^0_{AP} trends (Table 2). Thus, similar to what happened with H_2 solubility, solvent polarity is not considered a factor directing the AP hydrogenation rate, either.

It was previously verified that the solvent effect in the AP hydrogenation rate for each catalyst and the change of its magnitude among the three catalysts can be explained considering the nature and intensity of solvent-metal interactions [17]. In particular, CHX proved to have a very weak interaction with any of the three metal

Table 3
Concentration of H_2 in liquid phase and polarity parameters of the solvents.

Solvent	C_{H_2} (363 K) (mol/l)	ε[a]	μ[a] (D)	Z[a]	E_T (30) [a] (kcal/mol)	π^*[a]	α[a]	β[e]
IPA	3.24×10^{-2}[b]	19.9	1.66	76.3	49.2	0.48	0.76	0.84
CHX	3.72×10^{-2}[c]	2.02	0.00	60.1	30.9	0	0	0
TOL	3.76×10^{-2}[d]	2.38	0.37	56.1	33.9	0.54	0	0.11
BEN	3.81×10^{-2}[e]	2.28	0.00	54.0	34.3	0.59	0	0.10

[a] Obtained from Ref. [37].
[b] Obtained from Ref. [33].
[c] Obtained from Ref. [34].
[d] Obtained from Ref. [35].
[e] Obtained from Ref. [36].

surfaces, as it was determined in TPD experiments, since no CHX desorption was detectable on any catalysts (Fig. 6a–c). Thus the competition for the active metal sites between AP and this solvent would be negligible, making CHX appropriate to be used as a reference of a non-competitive solvent. On this basis, differences in catalytic activity in the other solvents can be attributed to the occurrence of surface phenomena such as promotion through hydrogen transfer and/or competition for active metal sites, as it was evidenced in hydrogen transfer tests and temperature programmed experiments carried out in this work.

When IPA was used as solvent, the initial hydrogenation rate was the highest with the three metal catalysts. In this case, two facts are acting to favor AP hydrogenation rate: (1) activation by polarization of C=O group in AP due to interaction with the C–OH group of IPA; (2) hydrogen transfer to AP from the dissociative adsorption of IPA on the metal surface. From the TPD experiments, it was concluded that an important interaction between IPA and the metal surface, decreasing noticeably from Ni/SiO_2 to Cu/SiO_2, leads to a significant amount of dissociatively chemisorbed hydrogen and weakly adsorbed IPA and acetone. The resulting effect is a hydrogen-rich metal surface that improves AP hydrogenation rates compared to those reached when CHX is used as solvent. Both the dissociative chemisorption of IPA and the hydrogen transfer ability are much more important with Ni/SiO_2 than with Co/SiO_2 and Cu/SiO_2 (Fig. 5 and Fig. 6d–f). Then, the highest activity of Co/SiO_2 and Cu/SiO_2 when IPA is used as solvent instead of CHX can mainly be explained by considering the polarization of AP molecules by interaction with IPA [38]. This polarization effect is also contributing to the AP hydrogenation rate on Ni/SiO_2. The sum of these two facts explain why the activity with IPA was higher than with CHX for the three catalyst and also explain the activity pattern across the metal series when IPA was used as solvent.

On the other hand, with BEN and TOL, the solvent-catalyst interactions have in general a negative influence on the AP hydrogenation rate respect to when CHX was used as solvent. This negative effect is varying noticeably with the metal nature, as mentioned above. In contrast with IPA, only competitive adsorption of BEN and TOL with AP for the active sites takes place, without any kind of promoting effect. The last is consistent with an irreversible adsorption of BEN and TOL over the metal surfaces, as it was verified in the TPD experiments (Fig. 6g–l). The grade of interaction of these solvents with metal surface follows the general trend: $Ni/SiO_2 > Co/SiO_2 > Cu/SiO_2$.

In the case of TOL, the solvent-catalyst interaction leads to irreversible adsorbed species (Fig. 6g–i), without generation of chemisorbed hydrogen. Thus, there is a competition for the active sites between AP and the irreversibly adsorbed species resulting from the TOL-catalyst interaction. This competition partially hampers the AP adsorption; hence the AP hydrogenation rate is some lower than in the case of CHX on each metal (Table 2).

Finally, the use of BEN as solvent gives the lowest catalytic activity in all the samples (Fig. 3 and Table 2). However, there are significant differences for the initial AP hydrogenation rate in BEN between Ni/SiO_2 (r^0_{AP} = 0 mol/h/g), Co/SiO_2 (r^0_{AP} = 6.36×10^{-3} mol/h/g) and Cu/SiO_2 (r^0_{AP} = 6.78×10^{-3} mol/h/g), which can be explained from the results obtained in TPD and TPH experiments. It was found that the interaction of BEN with the metal nickel surface is very strong and irreversible (Fig. 6j), even in the presence of H_2 (Fig. 7a). It is concluded that the coverage of the metal nickel surface with the strongly chemisorbed BEN leads to a complete blockage of the active nickel surface sites and the consequent total catalyst deactivation. In the case of Co/SiO_2, TPD experiments showed that there is a strong interaction between BEN and the metal cobalt surface, as well (Fig. 6k). However, it was clear that the amount of strongly chemisorbed BEN was much lower over Co/SiO_2 than over Ni/SiO_2 (Fig. 6j and k). As a consequence, for similar exposed metal surface, the coverage of metal surface on Co/SiO_2 would be lower than on Ni/SiO_2. Then, the initial AP hydrogenation rate on Co/SiO_2 was higher than zero and about the half of that estimated with CHX. TPH experiments after BEN adsorption on Ni/SiO_2 and Co/SiO_2 confirmed the existence of very strongly chemisorbed BEN but in very different amounts on each catalyst, thus supporting the TPD results. Finally, the interaction of BEN with Cu was very weak, as revealed by TPD and TPH (Fig. 6c and l and Fig. 7c). This explains why initial AP hydrogenation rate over Cu/SiO_2 either in CHX or BEN was quite similar (Table 2).

Solvent-metal interactions also influence the product distribution, though clearly in a lower degree than on the AP hydrogenation rate. For Ni/SiO_2 and Co/SiO_2 catalysts, which are more hydrogenolytic than Cu/SiO_2, the solvent-metal interaction leads in general to an increase of the maximum PHE yield, except when metal nickel was poisoned by BEN (Table 2). A plausible explanation of this increase in PHE yield is the blockage of a fraction of metal sites responsible for the PHE hydrogenolysis and/or ring hydrogenation. One support for this assumption was obtained from TPD experiments with IPA, TOL and BEN over Co/SiO_2 and Ni/SiO_2. In these experiments, the evolution of C_1 and C_2 fragments at $T > 500$ K coming from decomposition of strongly adsorbed IPA, TOL and BEN was observed. In the particular case of BEN, the strong adsorption over hydrogenolytic sites on Co/SiO_2 was more selective than on Ni/SiO_2. This led to an increase in PHE selectivity when Co/SiO_2 is used as catalyst. Instead, the non selective adsorption of BEN on Ni/SiO_2 leads to complete poisoning of metal Ni surface. Besides, with IPA, the interaction between C=O and C–OH groups might also favor the selective hydrogenation to PHE due to polarization of C=O group.

5. Conclusions

Important metal and solvent effects take place during the liquid-phase hydrogenation of acetophenone over silica-supported Ni-, Co- and Cu-based catalysts. In absence of strong solvent-metal interactions, the pattern for the initial acetophenone hydrogenation rate was: $Ni/SiO_2 > Co/SiO_2 > Cu/SiO_2$, whereas

the initial selectivity to 1-phenylethanol follows the trend: $Cu/SiO_2 \cong Co/SiO_2 > Ni/SiO_2$. The former patterns can be explained considering the capability for irreversible H_2 chemisorption, filling of *d* bands and ratio of attraction to repulsion forces between aromatic ring and metal surface. Instead, the maximum yield in 1-phenylethanol follows the pattern: $Cu/SiO_2 > Ni/SiO_2 > Co/SiO_2$. Thus, maximum yield in 1-phenylethanol decreases as metal activity for hydrogenolysis into ethylbenzene increases.

The solvent strongly influences the hydrogenation rate of acetophenone. Solvent interaction with metal surface can enhance or hamper the acetophenone hydrogenation rate. Particularly, dissociative chemisorption of 2-propanol increases hydrogenation rate of acetophenone through hydrogen transfer. Instead, in the case of benzene and toluene, acetophenone hydrogenation rate diminishes due to competitive adsorption of solvent with the reactant. In general, it was found that the initial hydrogenation rate of acetophenone depends on the solvent as it follows: 2-propanol > cyclohexane > toluene > benzene. However, the magnitude of the solvent effect depends on the metal nature and it diminishes following the pattern: Ni > Co > Cu. Thus, the most important hydrogen transfer from 2-propanol to acetophenone occurs with Ni/SiO_2. In the same way, interaction between benzene and metal nickel surface leads to complete poisoning of active phase. Instead, the smallest differences in activity and selectivity among solvents take place with Cu/SiO_2.

Both, metal and solvent effect can be explained analyzing the magnitude of the solvent-catalyst interactions. In this sense, useful information can be obtained from temperature programmed desorption of solvents, temperature programmed hydrogenation of solvents and hydrogen transfer tests. For 2-propanol, the ability of the catalyst to transfer hydrogen from the solvent to acetophenone shifts the conversion rate to the highest values following the same pattern than for metal activity. In addition, polarization of C=O group, by interaction with C–OH group, would also favor both hydrogenation rate of acetophenone and selectivity to 1-phenylethanol. If the solvent is not a hydrogen donor, the strength of the solvent-metal interaction rules the hydrogenation activity. In general, it was confirmed that the negative effect is much more important with benzene than with toluene.

Acknowledgments

We thank the Universidad Nacional del Litoral (UNL), Consejo Nacional de Investigaciones Científicas y Técnicas (CONICET), and Agencia Nacional de Promoción Científica y Tecnológica (ANPCyT), Argentina, for the financial support of this work.

References

[1] K. Bauer, D. Garbe, Ullmann's Encyclopedia, A11, third ed., VCH, New York, NY, 1988, pp. 141.
[2] P. Rylander, Hydrogenation Methods, Academic Press Inc, London, 1985, pp. 66.
[3] G.F. Santori, A.G. Moglioni, V. Vetere, G.Y. Moltrasio Iglesias, M.L. Casella, O.A. Ferretti, Appl. Catal., A 269 (2004) 215–223.
[4] C. Chen, H. Chen, W. Cheng, Appl. Catal., A 248 (2003) 117–128.
[5] L. Cerveny, Z. Belohlav, M.N.H. Hamed, Res. Chem. Intermed. 22 (1996) 15–22.
[6] M. Casagrande, L. Storaro, A. Talon, M. Lenarda, R. Frattini, E. Rodríguez-Castellón, P. Maireles-Torres, J. Mol. Catal. A: Chem. 188 (2002) 133–139.
[7] M.A. Aramendía, V. Borau, J.F. Gómez, A. Herrera, C. Jiménez, J.M. Marinas, J. Catal. 140 (1993) 335–343.
[8] A. Drelinkiewicza, A. Waksmundzka, W. Makowski, J.W. Sobczak, A. Król, A. Zięba, Catal. Lett. 94 (2004) 143–156.
[9] M. Bejblová, P. Zamostny, L. Cerveny, J. Cejka, Collect. Czech. Chem. Commun. 68 (2003) 1969–1984.
[10] J.M. Bonnier, J.P. Damon, J. Masson, Appl. Catal. A: Gen. 42 (1988) 285–297.
[11] J. Masson, S. Vidal, P. Cividino, P. Fouillox, J. Court, Appl. Catal., A 99 (1993) 147–159.
[12] J. Masson, P. Cividino, J. Court, Appl. Catal., A 161 (1997) 191–197.
[13] J. Masson, P. Cividino, J.M. Bonnier, P. Fouillox, Stud. Surf. Sci. Catal. 59 (1991) 245–252.
[14] M.V. Rajashekharam, I. Bergault, P. Fouilloux, D. Schweich, H. Delmas, R.V. Chaudhari, Catal. Today 48 (1999) 83–92.
[15] R.V. Malyala, C.V. Rode, M. Arai, S.G. Hegde, R.V. Chaudhari, Appl. Catal., A 193 (2000) 71–86.
[16] J.M. Bonnier, J. Court, P.T. Wierzchowski, Appl. Catal. A: Gen. 53 (1989) 217–231.
[17] N.M. Bertero, A.F. Trasarti, C.R. Apesteguía, A.J. Marchi, Appl. Catal., A 394 (2011) 228–238.
[18] F. Zaccheria, N. Ravasio, R. Psaro, A. Fusi, Tetrahedron Lett. 46 (2005) 3695–3697.
[19] N. Oku, M. Ishino, US Patent 6410806, Sumitomo Chemical Company, Japan, 2002.
[20] S. Ito, T. Hibi, US Patent 5663458, Sumitomo Chemical Company, Japan, 1997.
[21] N.M. Bertero, C.R. Apesteguía, A.J. Marchi, Appl. Catal., A 349 (2008) 100–109.
[22] N.M. Bertero, C.R. Apesteguía, A.J. Marchi, Catal. Today 172 (2011) 171–176.
[23] A. Dandekar, M.A. Vannice, J. Catal. 178 (1998) 621–639.
[24] A.J. Marchi, J.F. Paris, N.M. Bertero, C.R. Apesteguía, Ind. Eng. Chem. Res. 46 (2007) 7657–7666.
[25] P.A. Ramachandran, R.V. Chaudhari, Three Phase Catalytic Reactors, Gordon and Breach, New York, NY, 1983.
[26] P.B. Weisz, C.D. Prater, Adv. Catal. 6 (1954) 143–196.
[27] A.J. Marchi, J.I. di Cosimo, C.R. Apesteguía, Catal. Today 15 (1992) 383–394.
[28] A.F. Trasarti, A.J. Marchi, C.R. Apesteguía, J. Catal. 247 (2007) 155–165.
[29] A. Venugopal, S. Naveen Kumar, J. Ashok, D. Hari Prasad, V. Durga Kumari, K.B.S. Prasad, M. Subrahmanyam, Int. J. Hydrogen Energy 32 (2007) 1782–1788.
[30] F. Alonso, P. Riente, J.A. Sirvent, M. Yus, Appl. Catal., A 378 (2010) 42–51.
[31] F.-Z. Su, L. He, J. Ni, Y. Cao, H.-Y. He, K.-N. Fan, Chem. Commun. (2008) 3531–3533.
[32] F. Delbecq, P. Sautet, J Catal. 211 (2002) 398–406.
[33] J. Park, R.L. Robinson Jr., K.A.M. Gasem, J. Chem. Eng. Data 41 (1996) 70–73.
[34] E. Brunner, J. Chem. Eng. Data 30 (1985) 269–273.
[35] M. Herskowitz, J. Wisniak, L. Skladman, J. Chem. Eng. Data 28 (1983) 164–166.
[36] P. Lühring, A. Schumpe, J. Chem. Eng. Data 34 (1989) 250–252.
[37] Y. Marcus, Chem. Soc. Rev. 22 (1993) 409–416.
[38] J. Hájek, N. Kumar, P. Mäki-Arvela, T. Salmi, D.Yu. Murzin, J. Mol. Catal. A: Chem. 217 (2004) 145.